frontiers in Physics

ORIGINAL RESEARCH
published: 23 March 2022
doi: 10.3389/fphy.2022.869333

A Wideband Controllable Bandpass Filter Based on Spoof Surface Plasmon Polaritons

Xi Chen[1,2], *Chonghu Cheng*[1] *and Leilei Liu*[1]*

[1]College of Electronic and Optical Engineering, Nanjing University of Posts and Telecommunications, Nanjing, China, [2]School of Information Technology, Jiangsu Open University, Nanjing, China

A wideband controllable band-pass filter is proposed, which is based on the spoof surface plasmon polaritons (SSPP) and slip ring resonators (SRR). The design concept of the bandpass filter is using the SSPP and SRR to control the high cut-off frequency and filter the low-frequency wave, respectively. The bandpass filter is used diode reconfigurable technology to tunable the bandwidth. The filter has a passband range of 5–9 GHz, an out-band rejection of –20 dB for the lower sideband, and an out-band rejection of –50 dB for the upper sideband. The simulated and measured results are in good agreement over the operating band. Benefit from its low-profile and low-cost, the proposed bandpass filter has a great potential for development in plasmonic functional devices at microwave frequencies.

Keywords: bandpass filter, split ring resonators, spoof surface plasmon polaritons, reconfigurable technology, wideband

OPEN ACCESS

Edited by:
Zhewang Ma,
Saitama University, Japan

Reviewed by:
Yingjiang Guo,
University of Electronic Science and Technology of China, China
Zhen Liao,
Hangzhou Dianzi University, China

***Correspondence:**
Leilei Liu
liull@njupt.edu.cn

Specialty section:
This article was submitted to Optics and Photonics, a section of the journal Frontiers in Physics

Received: *04 February 2022*
Accepted: *28 February 2022*
Published: *23 March 2022*

Citation:
Chen X, Cheng C and Liu L (2022) A Wideband Controllable Bandpass Filter Based on Spoof Surface Plasmon Polaritons. Front. Phys. 10:869333. doi: 10.3389/fphy.2022.869333

INTRODUCTION

Due to the congestion in the lower frequency ranges, more occupancy of these regimes may cause interference, crosstalk and mutual coupling problem [1]. Meanwhile, compact integrated circuits with efficient energy, low loss and low crosstalk need to be investigated to satisfy the continuous development of wireless communication. Band pass filters (BPF) are one of the essential components of the wireless transceiver, thus designing a broadband BPF is important for RF circuit designers. Several structures have been reported in this regard [2, 3]. In literature [2], the BPF structures generated dual passband notches with the help of multiple stubs attached to patch. In literature [3], the BPF structures with multiple transmission zeros enable frequency response. However, most of the reported structures were of large circuit area and complex construction due to the use of vias or fabrication limitation. Therefore, a band pass filter based on the spoof surface plasmon polariton (SSPP) may be a good candidate for future microwave communications.

Surface plasmon polariton (SPP) is a class of special surface electromagnetic wave mode, which was used only in the optical region for a long time [4]. Pendry et al. [5]and Hibbins et al. [6]proposed that the metal embedding with periodic sub wavelength structures could also support SPP-like mode in lower frequencies, which is known as spoof SPP(SSPP). The SSPP has several advantages over conventional microwave devices, including limiting the microwave field in a sub-wavelength scale, rejecting electromagnetic (EM) interference, and having a wide bandwidth. In 2013, Shen and Cui [7] proposed a planar structure that could realize SSPP. After that, many planar SSPP structures employing printed circuit board (PCB) technology were presented in microwave region from C to K bands [8, 9]. Since then, some SSPP structures have been realized by modulating periodic holes or grooves on the metal surface in [10–16]. Meanwhile, some works on GaAs–based BPFs have been reported in

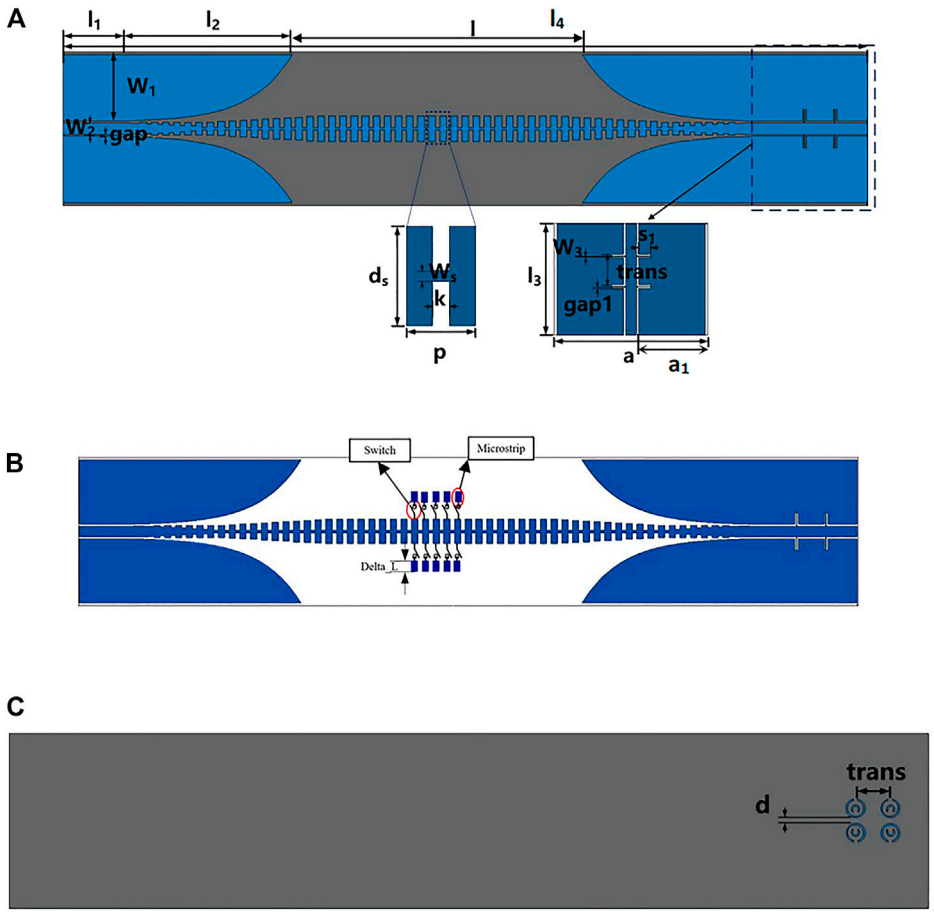

FIGURE 1 | (A) the front view of the spoof surface plasmon filter, **(B)** the front view of the spoof surface plasmon filter using diode reconfigurable technology, and **(C)** the back view of the spoof surface plasmon filter.

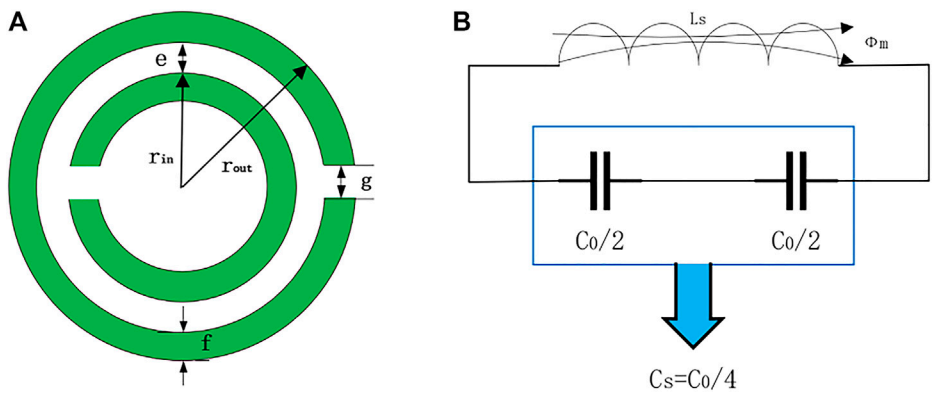

FIGURE 2 | (A) The structure of SRR, **(B)** the equivalent circuit diagram of the SRR structure.

recent years [17–19]. In [18], a bandpass filter with a notched band has good transmission performance was constructed. In [19], a new GaAs-based wideband SSPP waveguide with super compact size was presented.

Recently, several SSPP-based bandpass filters have been proposed [20–26]. Substrate integrated waveguides (SIWs) were used to achieve high-efficiency SSPP propagation with controlled lower cut-off frequencies, allowing for more tuning freedom [20–23].

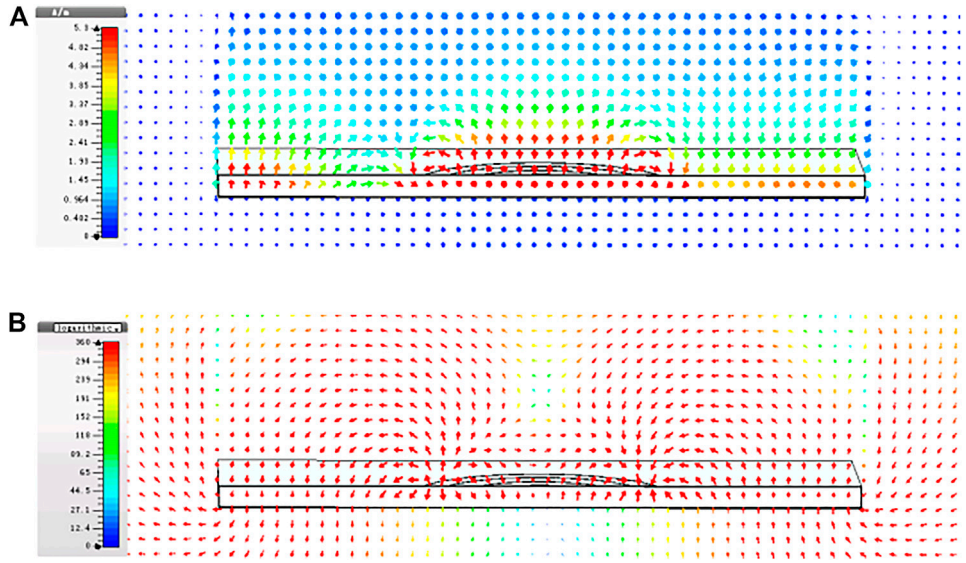

FIGURE 3 | (A) Simulation of electric field distribution of SRR at f = 4.75 GHz. **(B)** Simulation of magnetic field distribution of SRR at f = 4.75 GHz.

TABLE 1 | Parameter values of the SRR (unit: mm).

Parameter values of SRR (unit: mm)	
r_{out}	6
r_{in}	1
g	3
f	1
e	1.22

The SIW waveguide was directly coupled to the SSPP structure in literature [20], resulting in an extremely long physical length. In SIW, embedded SSPP units [21–23] were used to minimize the physical size. HMSIW was used to minimize the overall size of the filter in [24–26]. Using slotted HMSIW, a unit cell capable of supporting SSPP was proposed. The dispersion diagram, which is distinct from that of standard SSPP, may forecast both higher and lower cut-off frequencies in the passband. However, these designs were electronically adjustable, and changing the bandwidth is challenging. As a result, it is theoretically challenging to develop a planar mechanically controlled bandpass filter with separate controllability of low and high cut-off frequencies and low cost. Therefore, SSPP-based structures were a good choice for managing high cut-off frequency because of their advantages of having a high cut-off frequency that can be readily controlled by optimizing geometrical parameters [27–31]. Furthermore, some CPW- or microstrip-based coupling structures [32, 33]could be a promising candidate for controlling the low cut-off frequency following modification.

In this work, a wideband controllable bandpass filter is proposed, which is based on the SRR high-pass filter cascaded SSPP transmission line. The transmission characteristics own both the features of SRR and SSPP. The low-pass cut-off frequency can be controlled by SSPP structure, while the high-pass cut-off frequency can be controlled by SRR structure. The bandwidth can be tuned by diode reconfigurable technology. The filter has an operating passband over 5–9 GHz, an out-band rejection of −20 dB for the lower sideband, and an out-band rejection of −50 dB for the upper

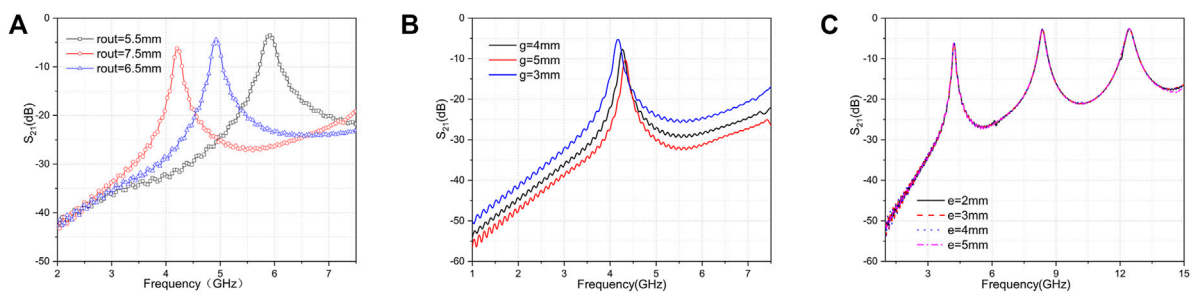

FIGURE 4 | (A) Analysis of the radius parameter r_{out} of the SRR outer ring. **(B)** Parameter analysis of the SRR ring opening spacing g. **(C)** Parameter analysis of the SRR ring opening spacing e.

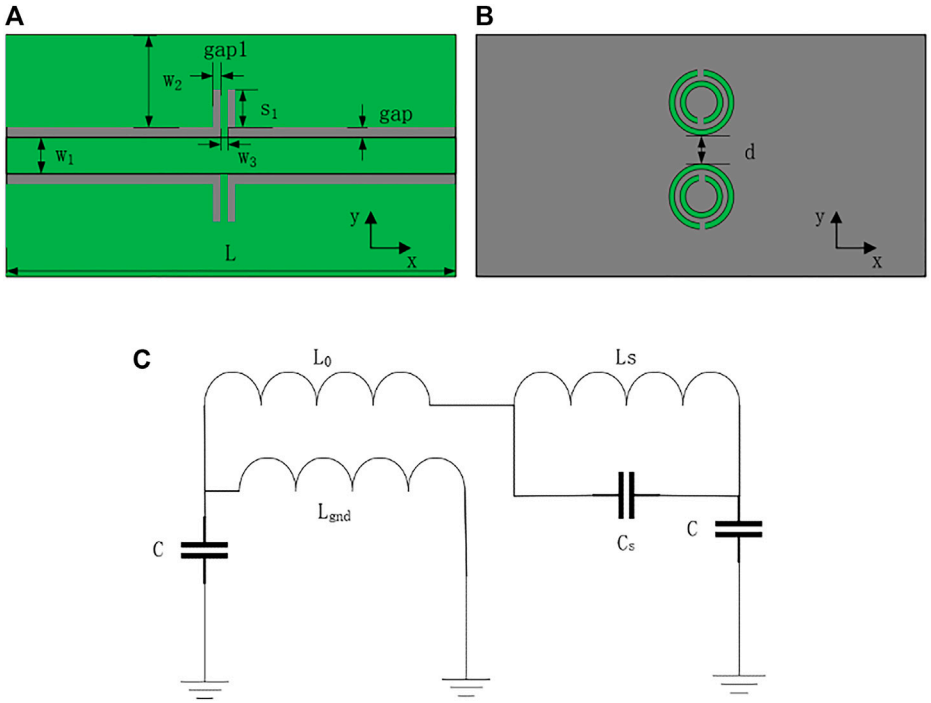

FIGURE 5 | Schematic diagram of bandpass filter based on SRR CPW structure. **(A)** The front side view **(B)** The back side view **(C)** Equivalent circuit of the SRR CPW structure.

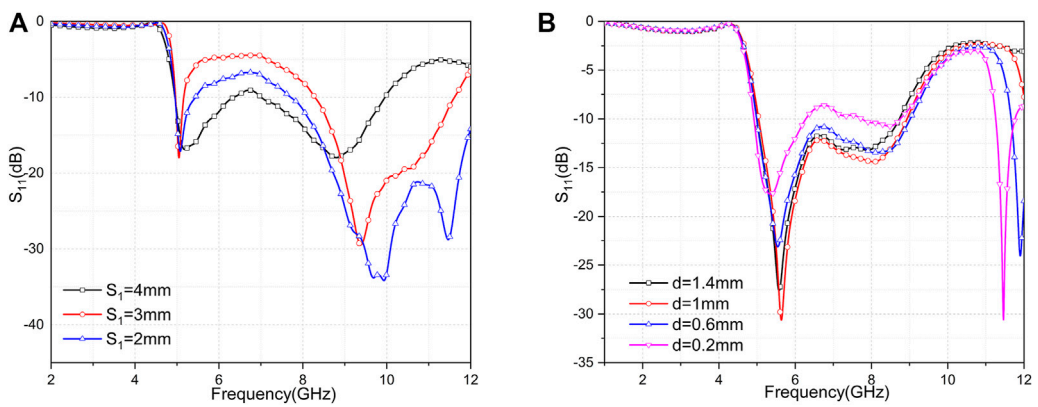

FIGURE 6 | (A) Performing sweep analysis on filter parameter S_1 **(B)** Performing sweep analysis on filter parameter *d*.

TABLE 2 | Parameter values of the bandpass filter with CPW structure based on SRR (unit: mm).

Parameter values of bandpass filter with CPW structure based on SRR (unit: mm)					
W_1	4	L	40	f	0.6
W_2	8.7	W_g	0.2	g	3
W_3	0.3	S_1	4.5	r_{in}	1.5
gap	0.3	d	1	r_{out}	3.2
gap_1	0.2	e	0.9	—	—

sideband. The physical processing is performed and verified, and the measured results agree well with the simulated results.

CONFIGURATION AND ANALYSIS

The bandpass filter is illustrated in **Figures 1A–C**. It can be considered as a combination of the SRR and SSPP units. The SSPP shown in **Figure 1A** controls the high cut-off frequency by changing the unit cell depth, while the SRR shown in **Figure 1C**

TABLE 3 | Parameters of bandpass filter with CPW structure based on SRR (unit: mm) (optimized).

Parameter values of bandpass filter with CPW structure based on SRR (unit: mm)					
W_1	4	L	43	f	0.62
W_2	32.7	W_g	0.7	g	1.454
W_3	0.3	S_1	4.5	r_{in}	1.28
gap	0.3	d	0.2	r_{out}	3.2
gap_1	0.2	e	1.92	—	—

TABLE 4 | Parameter values of SSPP filter.

Parameter values of SSPP filter (unit: mm)					
W_1	24	l_3	40	f	0.52
W_2	4	d_s	9.2	g	1.4
W_3	0.3	s_1	5	r_{in}	1.27
gap	0.7	d	1.83	r_{out}	3
gap_1	0.5	e	1.47	w_s	1
trans	11	p	6.4	k	1.6
l	290	a	53.4	l_2	44
l_1	10	l_4	182	a_1	24.7

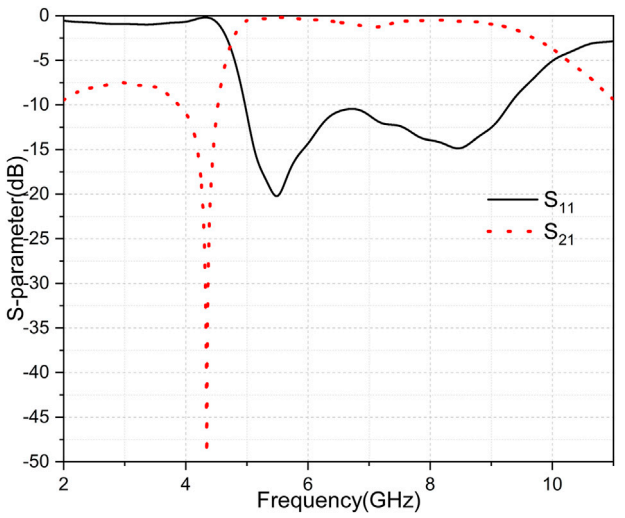

FIGURE 7 | Bandpass filter simulation results of SRR-based coplanar waveguide structure.

based coupling structure controls the low cut-off frequency by changing the width of grooves. In addition, the RF diodes in **Figure 1B** controlled by a DC power are added in the SSPP to regulate the bandwidth of passband.

The structure is printed on the 1 mm thick Taconic RF-35 substrate (relative permittivity $\varepsilon_r = 3.5$, loss tangent $\tan\delta = 0.001$). The SSPP is composed of a 50-Ω CPW transmission line using matched conversion. The width and length of SSPP uints are denoted by d_s and p, and the depth and width of grooves are denoted by w_s and k, respectively. The total width and length of the SSPP filter are marked as a and l, the access part is marked as l_1, CPW feeding part is marked as l_2, and the SRR part is marked as l_3. The gap width is marked as w_1, and the width of ground of CPW is marked as w_2. The length and width of the slotted slit are marked as s_1 and w_3, respectively. The slotted spacing is denoted by gap_1. Likewise, the distances between two SRR stages are denoted by *trans*, and the distances between two SRRs are denoted by d.

Configuration of Slip Ring Resonators

For the sake of clarity, the design of the bandpass filter starts with the basic bandpass filter, which consists of a CPW coupled with slip ring resonators (SRR). The structure of SRR is shown in **Figure 2A**. The coloring part is covered with a metal part, and its shape is the common center of two open rings spliced together. The currents will be induced in SRR when an external electromagnetic action received. The ring currents act as magnetic pole moments, which leads to the negative magnetic permeability. The coloring part of the figure is the copper-clad part, where r_{out} is the outer ring radius, e is the ring distance, f is the ring width, and r_0 is the average radius of the ring. These parameters are related to the main performance of the SRR. In a certain frequency range, this structure can be equivalent to the assembled element circuit diagram as shown in **Figure 2B**. C_0 is the equivalent capacitance between the whole ring and C_s is the series capacitance composed of the upper half and the lower half capacitances, which can be obtained from the series capacitance formula: $C_s = C_0/4$. L_s is the equivalent inductance of the SRR. The resonant frequency of the whole resonant circuit is given by

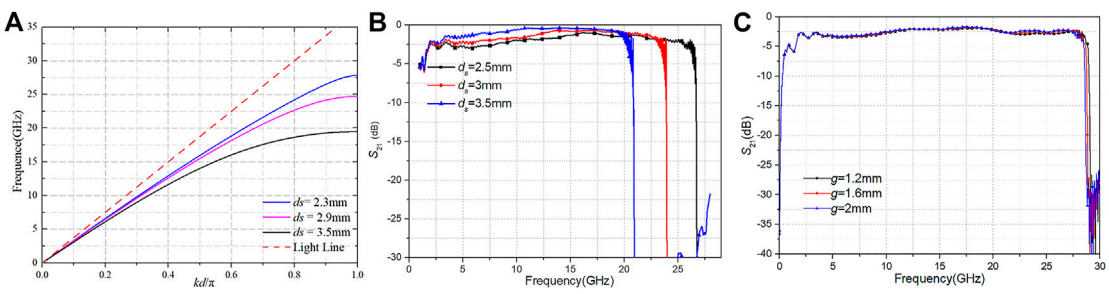

FIGURE 8 | (A) Dispersion performance of the SSPP-TL with different d_s. **(B)** S_{21} of the SSPP-TL with different d_s. **(C)** S_{21} of the SSPP-TL with different g.

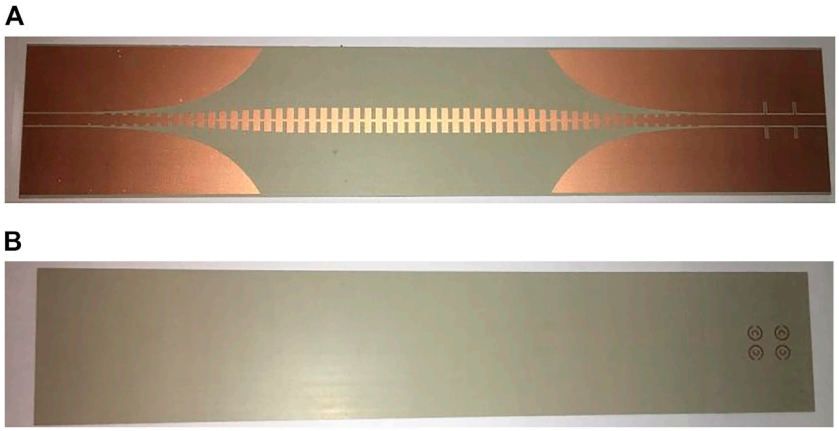

FIGURE 9 | The SSPP filter **(A)** front side **(B)** reverse side.

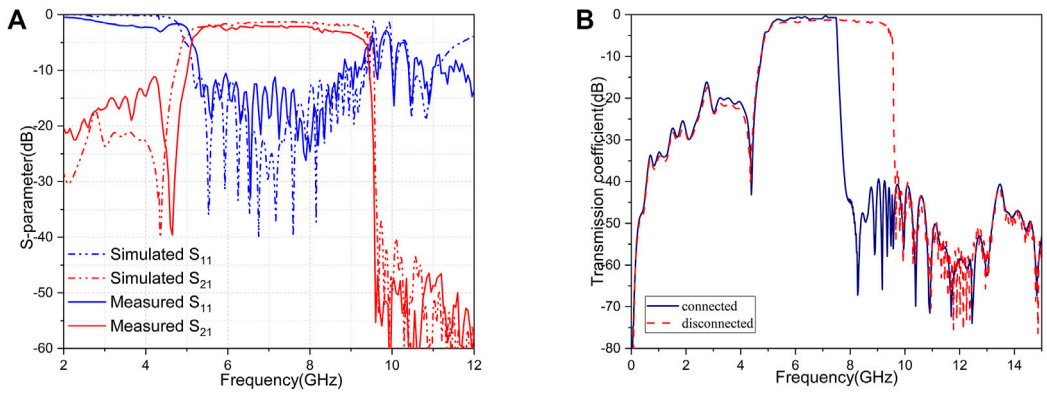

FIGURE 10 | (A) The *S*-parameters simulated and measured results of SSPP filter. **(B)** The transmission coefficient results of SSPP diode reconfigurable filter in **Figure 1B**.

TABLE 5 | Comparative study of the SSPP bandpass structure.

Ref.	BW/ GHz	Out-of-band rejection at low frequency	Out-of-band rejection at high frequency	Controllability of passband range
[9]	7.3–11.2	–30 dB	–40 dB	No
[15]	3–4.8	–30 dB	–30 dB	No
[19] A	3.6–7.1	–20 dB	–20 dB	No
[20]	0.6–1.5	–30 dB	–20 dB	No
[31]	7.3–10.5	–30 dB	–20 dB	No
This work	5–9.5	–40 dB	–50 dB	Yes

$$f = \frac{1}{2\pi\sqrt{L_s C_s}} \quad (1)$$

By structuring the SRR on the top of the dielectric substrate, the distributions of the electric field and the magnetic field are shown in **Figures 3A,B**, respectively. It can be observed that the electric- and magnetic-field distributions on the SRR symmetry surface are consistent.

From **Eq. 1**, the resonant frequency of the SRR is related to the ring radius. Because the inductance and the length are proportional, the length of the ring equivalent and the equivalent inductance L_s both increase with the raise of the ring radius. The dielectric substrate is Rogers RO4003C with the dielectric constant ε_r = 3.38, tanδ = 0.001, and thickness h = 1 mm. The Parameter values of the SRR is shown in **Table 1**.

The results simulated by the model *via* changing only the radius r_{out} of the outer ring of the SRR are shown in the **Figure 4**.

The resonant frequency is 4.23, 4.75, and 5.75 GHz for the SRR outer ring radius r_{out} = 7.5, 6.5, and 5.5 mm, respectively. It can be seen that the resonant frequency of the SRR decreases with the increase of the outer ring radius. When the SRR ring opening spacing g increases, the equivalent length increases and L_s decreases, thus the resonant frequency increases. Keeping the outer radius of the SRR ring as a constant of r_{out} = 7.5 mm, the simulation results are obtained for different SRR ring opening spacing g. From the above simulation curve sshown in **Figure 4B**, the resonant frequencies of SRR are 4.2, 4.25, and 4.3 GHz for the opening pitch gap of 3, 4, and 5 mm, respectively. The resonant frequency of SRR is shifted to the high

frequency direction with the increase of the ring opening pitch. If only the ring spacing e is changed without changing other parameters (g and r_{out}), the performance curves are obtained from the simulation shown in **Figure 4C**. From the analysis above, the effect of ring spacing e on the SRR is relatively small.

To complete the transition and achieve tight coupling, the coplanar waveguide (CPW) structure is placed on the front, the SRR resonant ring is symmetrically placed on the back, as shown in **Figures 5A,B**. This structure could produce a negative permeability effect near the resonant frequency to prevent the transmission of electromagnetic waves. The dimensions of the above structure are listed in **Table 2**. The equivalent circuit is shown in **Figure 5C**, where L_0 and C are the equivalent inductance and capacitance generated after the action of the SRR with CPW structure, respectively. L_s and C_s are the equivalent inductance and capacitance of the SRR after resonance generated in the structure, respectively. L_{gnd} represents the equivalent value of the grounding inductance. The series branch will change from inductive impedance to capacitive impedance. The port impedance is 50 Ω, which could matched to the SRR with CPW structure.

Keep the other parameters unchanged to perform simulations on parameters S_1 and d, the results in **Figure 6** could be obtained.

As shown in **Figure 6**, the passband bandwidth of the filter decreases when S_1 increases. This is mainly due to the increase of the ground inductance, which leads to the increase of the local resonant frequency. Simulations of parameter d show that the transmission characteristics in the passband gradually become better as d increases (the transmission coefficient S_{21} can be inferred from S_{11}). However, its transmission bandwidth remains basically unchanged, so we conclude that the passband bandwidth can be controlled by adjusting parameters S_1 and d to regulate the impedance matching in the passband. Finally, the dimensions of the above structure are derived by optimization, as shown in **Table 3**.

The scattering parameter (*S*-parameter) of the bandpass filter based on the SRR with CPW structure is shown in **Figure 7**. The *S*-parameter is obtained by simulating the model created by CST, and it produces good passband characteristics from 5 to 9 GHz as shown in **Figure 7**.

Configuration of Spoof Surface Plasmon Polaritons

The high frequency characteristics of the filter is based on the SSPP transmission line (TL). The SSPP unit dispersion curves are displayed in **Figure 8A**. These curves remain in the slow wave region, which are similar to the natural SPP material. The cutoff frequency decreases when the length of the slot increases. The wave number of the SSPP-TL unit is larger than that of the microstrip line, which suggests that the SSPP-TL unit has better electromagnetic constrain, lower coupling, and lower signal crosstalk than the microstrip line. In order to investigate the transmission loss performance of the SSPP-TL, the numerical simulation is performed, as shown in **Figure 8B**. The depth d_s of the trench determines the cutoff frequency of the SSPP-TL. As the cutoff frequency decreases, the transmission loss decreases due to the stronger electromagnetic field binding.

As shown in **Figure 8C**, the slot width g has almost no effect on the transmission properties. Therefore, the deeper the slot, the lower the cutoff frequency and the stronger its binding.

IMPLEMENTATION AND MEASUREMENT

Based on the theoretical analysis above, a bandpass filter with SSPP is designed. As shown in **Figure 9**, the SSPP based filter is cascaded by the SSPP transmission line and the SRR with CPW section. In the SRR with CPW section, the two-section SRR structure is used, which can effectively increase the low frequency rejection effect. The cutoff frequency of the SSPP TL is at 9.5 GHz. By adding a first-order ground inductor and SRR series structure, low-frequency stopband rejection can be achieved, and the optimized dimensions are listed in **Table 4**.

As shown in **Figure 10A**, the proposed SSPP filter has a good window characteristics. The passband range is 5~9.5GHz, the out-of-band rejection at 4 GHz is −20dB, and the out-of-band rejection at 10 GHz is −50dB for the bandpass filter. The measurement results and simulation results are basically consistent. Using reconfigurable technology, the passband range can be changed from 9.5 to 7.5 GHz by diode switching based on **Figure 10B**. A comparative study of the SSPP bandpass structures reported in recent literatures is presented in **Table 5**. The proposed filter features out-of-band rejection and passband range control.

CONCLUSION

In this paper, a wideband pandpass SSPP filter is proposed, which structured based on a SRR CPW section and a SSPP transmission line. The passband can be controlled by the RF diodes. The passband of proposed filter is range from 5 to 9.5 GHz, out-of-band rejection of -20 dB at 4 GHz, and out-of-band rejection of −50 dB at 10 GHz. The measurement results and simulation results are in agreement. Finally, a passband controllable filter using diode reconfigurable technology is proposed, and the simulation analysis is given to provide a new scheme for future filter design.

DATA AVAILABILITY STATEMENT

The original contributions presented in the study are included in the article/Supplementary Material, further inquiries can be directed to the corresponding author.

AUTHOR CONTRIBUTIONS

XC and LL contributed to this work equally. All authors listed have made a substantial, direct, and intellectual contribution to the work and approved it for publication.

FUNDING

This work was supported by the Natural Science Foundation of China under Grant 62001250.

REFERENCES

1. Otsuji T, Shur M. Terahertz Plasmonics: Good Results and Great Expectations. *IEEE Microwave* (2014) 15(7):43–50. doi:10.1109/MMM.2014.2355712
2. Ghazali AN, Sazid M, Pal S. A Compact Broadside Coupled Dual Notched Band UWB-BPF with Extended Stopband. *AEU - Int J Electron Commun* (2017) 82: 502–7. doi:10.1016/j.aeue.2017.10.021
3. Ghazali AN, Sazid M, Pal S. Multiple Passband Transmission Zeros Embedded Compact UWB Filter Based on Microstrip/CPW Transition. *AEU - Int J Electron Commun* (2021) 129(1):153549. doi:10.1016/j.aeue.2020.153549
4. Barnes WL, Dereux A, Ebbesen TW. Surface Plasmon Subwavelength Optics. *Nature* (2003) 424(6950):824–30. doi:10.1038/nature01937
5. Pendry JB, Marti´n-Moreno L, Garcia-Vidal FJ. Mimicking Surface Plasmons with Structured Surfaces. *Science* (2004) 305(5685):847–8. doi:10.1126/science.1098999
6. Hibbins AP, Evans BR, Sambles JR. Experimental Verification of Designer Surface Plasmons. *Science* (2005) 308(5722):670–2. doi:10.1126/science.1109043
7. Shen X, Jun Cui T. Planar Plasmonic Metamaterial on a Thin Film with Nearly Zero Thickness. *Appl Phys Lett* (2013) 102(21):211909. doi:10.1063/1.4808350
8. Lei W, Che W, Deng K, Dong S. Narrow-Slot Bandpass Filter Based on Folded Substrate-Integrated Waveguide with Wide Out-Of-Band Rejection. *Microw Opt Technol Lett* (2008) 50:1155–9. doi:10.1002/mop.23327
9. Yang T, Chi P-L, Xu R, Lin W. Folded Substrate Integrated Waveguide Based Composite Right/Left-Handed Transmission Line and its Application to Partial H-Plane Filters. *IEEE Trans Microwave Theor Techn.* (2013) 61(2):789–99. doi:10.1109/TMTT.2012.2231431
10. Yu L-Z, Yuan C-W, He J-T, Zhang Q. Beam Steerable Array Antenna Based on Rectangular Waveguide for High-Power Microwave Applications. *IEEE Trans Plasma Sci* (2019) 47(1):535–41. doi:10.1109/TPS.2018.2884290
11. Feng W, Ma X, Shi Y, Shi S, Che W. High-Selectivity Narrow- and Wide-Band Input-Reflectionless Bandpass Filters with Intercoupled Dual-Behavior Resonators. *IEEE Trans Plasma Sci* (2020) 48(2):446–54. doi:10.1109/TPS.2020.2968481
12. Zhuang Z, Wu Y, Yang Q, Kong M, Wang W. Broadband Power Amplifier Based on a Generalized Step-Impedance Quasi-Chebyshev Lowpass Matching Approach. *IEEE Trans Plasma Sci* (2020) 48(1):311–8. doi:10.1109/TPS.2019.2954494
13. Kong M, Wu Y, Zhuang Z, Wang W, Wang C. Ultraminiaturized Wideband Quasi-Chebyshev/-Elliptic Impedance-Transforming Power Divider Based on Integrated Passive Device Technology. *IEEE Trans Plasma Sci* (2020) 48(4): 858–66. doi:10.1109/TPS.2020.2980029
14. Zhou K, Zhou C-X, Wu W. Substrate-Integrated Waveguide Dual-Mode Dual-Band Bandpass Filters with Widely Controllable Bandwidth Ratios. *IEEE Trans Microwave Theor Techn.* (2017) 65(10):3801–12. doi:10.1109/TMTT.2017.2694827
15. Liu L, Jiang Y, Hu Y, Jiang D, Zhu L. Wideband Millimeter-Wave Endfire Antenna Based on Symmetrical Spoof Surface Plasmon Polaritons. *IEEE Trans Antennas Propagat* (2021) 69(11):7386–93. doi:10.1109/TAP.2021.3076199
16. Jiang Y, Liu L, Hu Y, Jiang D. Wideband Small Aperture Endfire Antenna Based on Spoof Surface Plasmon Polaritons. *IEEE Trans Antennas Propagat* (2021) 69(8): 5026–31. doi:10.1109/TAP.2021.3060141
17. Guo Y-J, Xu K-D, Deng X, Cheng X, Chen Q. Millimeter-Wave On-Chip Bandpass Filter Based on Spoof Surface Plasmon Polaritons. *IEEE Electron Device Lett* (2020) 41(8):1165–8. doi:10.1109/LED.2020.3003804
18. Xu K-D, Lu S, Guo Y-J, Chen Q. High-Order Mode of Spoof Surface Plasmon Polaritons and its Application in Bandpass Filters. *IEEE Trans Plasma Sci* (2021) 49(1):269–75. doi:10.1109/TPS.2020.3043889
19. Xu K-D, Guo Y-J, Yang Q, Zhang Y-L, Deng X, Zhang A, et al. On-Chip GaAs-Based Spoof Surface Plasmon Polaritons at Millimeter-Wave Regime. *IEEE Photon Technol Lett* (2021) 33(5):255–8. doi:10.1109/LPT.2021.3054962
20. Guan D-F, You P, Zhang Q, Xiao K, Yong S-W. Hybrid Spoof Surface Plasmon Polariton and Substrate Integrated Waveguide Transmission Line and its Application in Filter. *IEEE Trans Microwave Theor Techn.* (2017) 65(12): 4925–32. doi:10.1109/TMTT.2017.2727486
21. Chen P, Li L, Yang K, Chen Q. Hybrid Spoof Surface Plasmon Polariton and Substrate Integrated Waveguide Broadband Bandpass Filter with Wide Out-Of-Band Rejection. *IEEE Microw Wireless Compon Lett* (2018) 28(11):984–6. doi:10.1109/LMWC.2018.2869290
22. Ye L, Chen Y, Xu KD, Li W, Liu QH, Zhang Y. Substrate Integrated Plasmonic Waveguide for Microwave Bandpass Filter Applications. *IEEE Access* (2019) 7: 75957–64. doi:10.1109/ACCESS.2019.2920925
23. Zhang D, Zhang K, Wu Q, Jiang T. Efficient Propagation of Spoof Surface Plasmon Polaritons Supported by Substrate Integrated Waveguide with Bandpass Features. *J Phys D: Appl Phys* (2020) 53(42):425104. doi:10.1088/1361-6463/ab9f6a
24. Cui Y, Xu K-D, Guo Y-J, Chen Q. Half-Mode Substrate Integrated Plasmonic Waveguide for Filter and Diplexer Designs. *J Phys D: Appl Phys* (2022) 55(12): 125104. doi:10.1088/1361-6463/ac44bf
25. Zhang D, Zhang K, Wu Q, Jiang T. A Compact Wideband Filter Based on Spoof Surface Plasmon Polaritons with a Wide Upper Rejection Band. *IEEE Photon Technol Lett* (2020) 32(24):1511–4. doi:10.1109/LPT.2020.3029290
26. Guo Y-J, Xu K-D, Deng X, Cheng X, Chen Q. Millimeter-Wave On-Chip Bandpass Filter Based on Spoof Surface Plasmon Polaritons. *IEEE Electron Device Lett* (2020) 41(8):1165–8. doi:10.1109/LED.2020.3003804
27. Zhang HC, He PH, Gao X, Tang WX, Cui TJ. Pass-Band Reconfigurable Spoof Surface Plasmon Polaritons. *J Phys Condens Matter* (2018) 30(13):134004. doi:10.1088/1361-648X/aaab85
28. Zhou YJ, Yang BJ. Planar Spoof Plasmonic Ultra-Wideband Filter Based on Low-Loss and Compact Terahertz Waveguide Corrugated with Dumbbell Grooves. *Appl Opt* (2015) 54(14):4529–33. doi:10.1364/AO.54.004529
29. Ma HF, Shen X, Cheng Q, Jiang WX, Cui TJ. Broadband and High-Efficiency Conversion from Guided Waves to Spoof Surface Plasmon Polaritons. *Laser Photon Rev* (2014) 8(1):146–51. doi:10.1002/lpor.201300118
30. Zhao L, Zhang X, Wang J, Yu W, Li J, Su H, et al. A Novel Broadband Band-Pass Filter Based on Spoof Surface Plasmon Polaritons. *Sci Rep* (2016) 6(1): 36069. doi:10.1038/srep36069
31. Zhang W, Zhu G, Sun L, Lin F. Trapping of Surface Plasmon Wave through Gradient Corrugated Strip with Underlayer Ground and Manipulating its Propagation. *Appl Phys Lett* (2015) 106:021104. doi:10.1063/1.4905675
32. Abbosh A, Ibrahim S, Karim M. Ultra-Wideband Crossover Using Microstrip-To-Coplanar Waveguide Transitions. *IEEE Microw Wireless Compon Lett* (2012) 22(10):500–2. doi:10.1109/LMWC.2012.2218586
33. Wang J, Zhao L, Hao Z-C. A Band-Pass Filter Based on the Spoof Surface Plasmon Polaritons and CPW-Based Coupling Structure. *IEEE Access* (2019) 7:35089–96. doi:10.1109/ACCESS.2019.2903147

Conflict of Interest: The authors declare that the research was conducted in the absence of any commercial or financial relationships that could be construed as a potential conflict of interest.